J. Fluid Mech. (1988), *vol.* 189, *pp.* 553–569
Printed in Great Britain

Electrically driven vortices in a strong magnetic field

By JOËL SOMMERIA
Madylam, Institute de Mécanique de Grenoble, BP 95,
38402 Saint-Martin D'Hères Cedex, France

(Received 14 November 1985 and in revised form 5 October 1987)

A steady isolated vortex is produced in a horizontal layer of mercury (of thickness a), subjected to a uniform vertical magnetic field. The vortex is forced by an electric current going from an electrode in the lower plane to the circular outer frame. The flow is investigated by streak photographs of small particles following the free upper surface, and by electric potential measurements. The agreement with the asymptotic theory for high values of the Hartmann number M is excellent for moderate electric currents. In particular all the current stays in the thin Hartmann layer of thickness a/M, except in the vortex core of horizontal extension $a/M^{\frac{1}{2}}$. For higher currents, the size of the core becomes larger and depends only on the local interaction parameters. When the current is switched off, we measure the decay due to the Hartmann friction. A similar study is carried out for a vortex created by an initial electric pulse, and for a pair of vortices of opposite sign. For all these examples, the dynamics can be described by the two-dimensional Navier–Stokes equations with Hartmann friction, except in the vortex cores. Finally a vortex is produced near a lateral wall and a detachment of the boundary layer parallel to the magnetic field occurs, by which a second vortex of opposite sign is generated.

1. Introduction

The theory of rectilinear laminar duct flows of a conducting fluid in a transverse uniform magnetic field is well understood and has been tested experimentally, and the topic is reviewed by Hunt & Shercliff (1971) and Shercliff (1975). This theory can be extended to three-dimensional flows at high Hartmann number, when the electromagnetic forces dominate the advective effects. However only a few situations have been investigated experimentally. Circular flows between two concentric cylinders, driven by a radial electric current, were studied by Baylis (1971) and Tabeling & Trakas (1984). The circular jet obtained between two concentric annular electrodes in an axial magnetic field was investigated by Lehnert (1952). A double chain of two-dimensional vortices was then observed as the result of an instability. Another kind of jet was obtained by Hunt & Malcolm (1968) and Malcolm (1970) around two circular electrodes set opposite to each other in an axial magnetic field, while the current was confined to the cylinder of fluid joining the two electrodes.

The present paper deals with new examples of flows at high Hartmann number, involving a vortex created by the interaction of the magnetic field with the current injected at an electrode. The experimental device and the method of measurement are described in §2. We report in §4.1 an experimental study of a single steady vortex, in which the electric steady forcing is balanced by the Hartmann friction. We consider in §4.2 the decay of this vortex by the Hartmann friction when the current

is switched off. Another kind of decaying vortex, generated by a short current pulse, is described in §4.3. A pair of two such vortices of opposite sign with a translating motion is studied in §4.4. Finally we consider in §4.5 the interaction of a vortex with a lateral wall, which involves a detachment of the boundary layer parallel to the magnetic field. The experimental data are compared to the corresponding theoretical results of §3, obtained by assuming that the electromagnetic effects on a typical three-dimensional eddy dominate the viscous and advective effects.

The important feature of the situations that we consider here is the existence of a two-dimensional bulk flow in the plane perpendicular to the magnetic field, outside the thin boundary layers. The only electromagnetic effects on these two-dimensional flows is the Hartmann friction and the forcing due to the injected currents. These effects are fairly weak, so that the inertia of the flow is important, even in a strong magnetic field. Since by contrast the three-dimensional flows are generally quickly damped by the eddy currents, these two-dimensional flows should be the only ones to survive. We can expect to observe them preferentially when they are allowed by the boundary conditions. This is the case in a fluid limited by two insulating planes perpendicular to the magnetic field. A well-known example is the persistence of strong residual turbulence in duct flows with a rectangular cross-section submitted to a transverse magnetic field (Lielausis 1975; Branover 1978; Branover & Gershon 1979). Kolesnikov & Tsinober (1974) have studied two-dimensional turbulence generated by a grid in a similar duct. The same idea underlies an investigation of two-dimensional turbulence produced in a confined layer of mercury by Sommeria (1986) and Verron & Sommeria (1987). These studies are summarized, with some of the results presented here, in Sommeria (1985).The flow was electrically driven by a lattice of electrodes, each acting in the same way as in the present work. However, we deal here with much simpler flows and the magnetohydrodynamic aspect can be studied in detail.

2. The experimental device

A vertical magnetic field between 0 and 1 tesla, with a uniformity better than 1 %, is provided by an electromagnet in a gap of thickness 6 cm and section 20×56 cm^2. The main apparatus is a closed circular box with an inner diameter of 12 cm containing a horizontal layer of mercury (Figure 1). The bottom is made of an insulating plate at the centre of which a circular copper electrode is inserted flush (diameter 2.5 mm). The outer frame is a thick copper ring that can be considered as infinitely conducting. The top cover is made of transparent acrylic. Velocity is kept small enough (< 10 cm/s), for the deformation of the upper surface to be negligible. Great care is necessary to avoid mercury pollution in order to keep a really free upper surface. For this purpose we use distilled mercury of good purity and maintain a permanent pressure of nitrogen (U quality) inside the box. Furthermore the bottom is covered with polypropylene and the copper parts are protected by a chemical nickel layer (50 μm thick) with a very thin electrolytic gold coating. The gold is dissolved at the first contact with mercury but the underlying nickel is then very clean and the electric contact excellent: the contact resistance is less than $10^{-3}\ \Omega/\text{mm}^2$. The walls are highly polished to avoid perturbations of the boundary layers. The temperature is maintained constant at 14 °C$\pm$1 °C by the iron of the electromagnet and its cooling circuit. Under these conditions the viscosity of mercury is $\nu = 1.17 \pm 0.1\ 10^{-7}\ \text{m}^2\,\text{s}$, the density $\rho = 1.355\ 10^4\ \text{kg m}^{-3}$, and conductivity $\sigma = (1.05 \pm 0.002)\ 10^6\ \Omega^{-1}\ \text{m}^{-1}$.

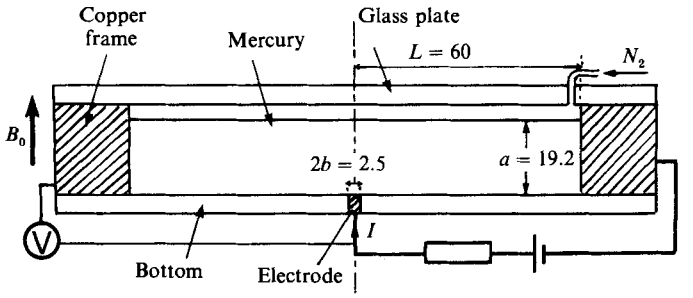

FIGURE 1. Cross-section of the circular tank with a schematic representation of the current supply and device for potential measurement. Dimensions are indicated in mm.

The flow is investigated by two methods. We get the velocity field by measuring the short streaks of aluminized rilsan particles 50 μm in diameter, which follow the free surface. These particles are sprinkled on mercury (in an argon atmosphere) before we close the box and remain there for the full series of experiments. Lateral illumination is provided by two sets of optic fibres. The time of exposure is precisely controlled by an external electrically driven diaphragm shutter. Because of the presence of the electromagnet above the free surface, a 45° mirror is used, and we can only visualize a band 2 cm wide at any one time. The second method is the measurement of the potential difference between the electrode and the outer frame. This low voltage (< 1 mV) is amplified 5000 times by an operational amplifier and most of the noise is eliminated by a low-pass filter. A minimum voltage variation of 0.5 μV can be detected.

In addition to this circular box, a similar square box of side 12 cm, described by Sommeria (1986), with a bottom containing a periodic network of 36 electrodes, is used to generate one or two isolated vortices by current pulses and to study their evolution.

3. Theory

3.1. *The approximation of strong magnetic fields*

We consider the fluid confined between two horizontal planes whose equations are $z = 0$ and $z = a$, with respect to a set of Cartesian coordinates x, y, z. We suppose that the magnetic Reynolds number is small, which means that the magnetic field $\boldsymbol{h}$ produced by the electric currents is negligible compared to the uniform vertical magnetic field $\boldsymbol{B}_0$ generated by the electromagnet. The equations of magneto-hydrodynamics for an incompressible velocity field $\boldsymbol{v}$ are then (see for example Shercliff 1965).

$$\Delta \boldsymbol{h} = -\mu_0 \sigma B_0 \frac{\partial \boldsymbol{v}}{\partial z}, \tag{1}$$

$$\frac{\mathrm{d}\boldsymbol{v}}{\mathrm{d}t} = \nu \Delta \boldsymbol{v} - \frac{\nabla P'}{\rho} + \left(\frac{B_0}{\mu_0 \rho}\right) \frac{\partial \boldsymbol{h}}{\partial z}, \tag{2}$$

$$\nabla \cdot \boldsymbol{v} = 0, \quad \nabla \cdot \boldsymbol{h} = 0, \tag{3}$$

where $\mathrm{d}/\mathrm{d}t = \partial/\partial t + \boldsymbol{v} \cdot \nabla$ and $\boldsymbol{h}$ is related to the density of electric current $\boldsymbol{j}$ by

$$\mu_0 \boldsymbol{j} = \nabla \times \boldsymbol{h}. \tag{4}$$

We shall also need Ohm's law to calculate the electric potential Φ

$$\boldsymbol{j} = \sigma(-\boldsymbol{\nabla}\Phi + \boldsymbol{v}\times\boldsymbol{B}_0). \tag{5}$$

The domain of strong magnetic fields is characterized by large values of the Hartmann number M and of the interaction parameter N defined by

$$M = (\sigma/\rho\nu)^{\frac{1}{2}} B_0 a, \quad N = (\sigma B_0^2/\rho)\, a/U,$$

where U is a typical velocity scale. The square of the Hartmann number and the interaction parameter can be considered as the ratio of the effect of the eddy currents (upon a typical three-dimensional initial state) to the viscous and to the advective forces respectively. In a strong magnetic field, the flow can be split into a core where vertical derivatives are weak, and a thin Hartmann layer of thickness a/M at the bottom of the box, matching the outer flow with zero velocity at the wall. A different kind of boundary layer, parallel to the magnetic field, lies along the lateral walls. Shear layers also arise from the electrical discontinuities at the edge of the electrodes, and follow the magnetic field lines. The thickness of these two kinds of layers is of the order of $a/M^{\frac{1}{2}}$ for slow flows but can be enlarged by advective effects at higher velocities and their thickness can then depend on the interaction parameter. Various kinds of advective effects have been studied by Hunt & Leibovich (1967), Kapila & Ludford (1977), Tabeling & Chabrerie (1981).

In the Hartmann layer the z derivatives greatly exceed the transverse derivatives, so one can neglect, to a first approximation, all the terms which do not involve z derivatives in (1) to (3). The new equations can be integrated easily with respect to the z variable, taking into account the condition of zero velocity at the bottom plane $z = 0$.

$$\boldsymbol{v}_\perp(x, y, z, t) = (1 - \mathrm{e}^{-zM/a})\, \boldsymbol{V}(x, y, t), \tag{6}$$

$$\boldsymbol{h}_\perp(x, y, z, t) = -\alpha \boldsymbol{V}(x, y, t)\, \mathrm{e}^{-zM/a} + \boldsymbol{h}_1(x, y, t), \tag{7}$$

$$v_z = 0, \quad h_z = h_z(x, y, t), \tag{8}$$

where $\alpha = \mu_0(\rho\nu\sigma)^{\frac{1}{2}}$ and the horizontal projection of a vector is denoted by the subscript $\perp$. Using (7) and neglecting the horizontal derivatives of $\boldsymbol{h}$ with respect to the vertical ones, the three components of (4) yield on the bottom plate

$$\boldsymbol{j}_{\perp(z=0)} = -\alpha M/a\, \boldsymbol{V}\times\boldsymbol{B}_0/B_0, \tag{9}$$

$$\boldsymbol{\nabla}\times\boldsymbol{h}_1 = \mu_0 j_{z(z=0)}\, \boldsymbol{B}_0/B_0 + \alpha\boldsymbol{\nabla}\times\boldsymbol{V}. \tag{10}$$

The vector $\boldsymbol{j}_\perp$ vanishes at the electrodes, considered as infinitely conducting, so that $\boldsymbol{V} = \boldsymbol{0}$ there. By contrast $j_{z(z=0)}$ is equal to the current density injected through the electrode surface and vanishes on the insulating areas.

In the limit of strong magnetic fields, (1) and (2) state that the vertical derivatives of $\boldsymbol{v}$ and $\boldsymbol{h}$ are small outside the Hartmann layers. A flow structure consistent with (1) to (3) is then a two-dimensional velocity field, for which velocity and magnetic field must be matched with the upper region of the Hartmann layer. The two-dimensional bulk flow must then be assimilated to $\boldsymbol{V}(x, y, t)$ and the following relations are obtained

$$\left.\begin{array}{ll} \mathrm{d}\boldsymbol{V}/\mathrm{d}t = \nu\Delta\boldsymbol{V} - \boldsymbol{\nabla}P/\rho + \boldsymbol{f}(x, y, t) - \boldsymbol{V}/t_{\mathrm{H}} & \text{outside the electrodes,} \\ \boldsymbol{V} = \boldsymbol{0} & \text{above the electrodes,} \end{array}\right\} \tag{11}$$

$$\boldsymbol{h} = (\mu_0\rho a/B_0)\,(z/a - 1)\,(\boldsymbol{f} - \boldsymbol{V}/t_{\mathrm{H}}), \tag{12}$$

$$\boldsymbol{\nabla}\times\boldsymbol{f} = -j_z(x, y, t)\,(\boldsymbol{B}_0/\rho a). \tag{13}$$

This flow satisfies the condition of a free upper surface, so a boundary layer is not required at the plane $z = a$. The electromagnetic effects on the two-dimensional flow are a linear friction term with a characteristic time $t_H = (\rho/\sigma\nu)^{\frac{1}{2}} a/B_0$ and a vorticity source or sink proportional to the electric current j_z. Physically, the corresponding driving force is due to the horizontal projection $\boldsymbol{J}_\perp$ of the injected current integrated along a vertical line. The curl of this force $\boldsymbol{J}_\perp \times \boldsymbol{B}_0$ is equal to $-(\boldsymbol{\nabla}\cdot\boldsymbol{J}_\perp)\boldsymbol{B}_0$. Because of the current conservation, $\boldsymbol{\nabla}\cdot\boldsymbol{J}_\perp$ is equal to the current density through the bottom, which leads again to (13). The driving force $\boldsymbol{f}$ is defined from (10) only by its curl, so that the pressure in (11) does not need to be the same as in (2). Notice that $\boldsymbol{J}_\perp \times \boldsymbol{B}_0$ is non-divergent everywhere, and the Hartmann friction as well, so that the physical pressure must be P instead of P'.

The velocity field of (11) is discontinuous at the edge of the electrodes. The flows over conducting and insulating areas must be matched by a shear layer parallel to the field, where (1) has to be used without approximation. This calculation is carried out in §3.3 for the simple case of an axisymmetric electrically driven vortex, when the velocity is small enough for the secondary radial flows to be negligible.

3.2. *Stability of the Hartmann layer and outer flow*

We have described a class of asymptotic solutions of the MHD equations with a thin Hartmann layer and a quasi-two-dimensional core. To have a physical reality, this structure of the flow should not be modified by the growth of small perturbations. Two kinds of instabilities could be expected according to whether the Hartmann layer or the core of the flow is concerned.

Lock (1955) has calculated that the Hartmann layer in a duct is unstable to infinitesimal perturbations for values of the parameter Re/M larger than 50000. The corresponding amplified perturbations have a small scale of the order of the Hartmann-layer thickness, and are only weakly affected by the magnetic field. The stability problem is then nearly identical to that of an ordinary boundary layer with an exponential profile of the same thickness (obtained with a suction at the wall). Indeed the parameter Re/M is nothing other than the Reynolds number calculated with the layer thickness. In practice, the rectangular duct flows are found to be turbulent for values of Re/M higher than 250 (Hua & Lykoudis 1974), so the Hartmann layer is unstable to perturbations of finite amplitude much below the threshold of the linear stability theory. In fact considerable turbulent fluctuations are still observed for values of Re/M below 250, although the pressure losses correspond to the laminar law. However these fluctuations are generated at the duct entrance or upstream and survive for a long time because of their two-dimensional dynamics (Branover & Gershon 1979), so they do not involve any instability of the Hartmann layer. Indeed such fluctuations are not observed in an annular (electrically driven) duct flow entirely embedded in the magnetic field (Gel'fat *et al.* 1971). Thus we can consider in practice that the condition

$$Re/M = M/N = (\rho/\sigma\nu)^{\frac{1}{2}} U/B < 250, \tag{14}$$

must be satisfied for the Hartmann layer to be laminar and to be described by (6)–(8). This condition is satisfied in all the experiments that we report here.

The possible growth of three-dimensional perturbations in the two-dimensional bulk depends of course on each particular flow. General guidelines can however be obtained by assuming that the different perturbed horizontal planes interact only by electromagnetic effects, which is likely to be true in a strong magnetic field (Alemany

et al. 1979). The growth of three-dimensional perturbations can be then related to the unpredictability of the two-dimensional motions. This idea lead Sommeria & Moreau (1982) to propose that the flow structures with a large horizontal size should stay two-dimensional, while the smaller structures become three-dimensional. The transition between these two behaviours corresponds to a length proportional to $aN^{-\frac{1}{3}}$, the coefficient of proportionality depending on the particular flow structure. Since the flows that we are considering here are not chaotic, the decorrelations in the different planes should not grow fast and the scale of transition should be small. Possible instabilities are likely to be restricted to the parallel shear layers.

3.3. *An electrically driven vortex*

A steady current I flows from the central electrode to the frame through the fluid, stimulating it into a circular motion (figure 2). This situation can be first analysed by the two-dimensional equation (11) and relation (13). If viscosity is neglected, a steady axisymmetric solution is immediately obtained for the azimuthal velocity component v_θ

$$v_\theta = \Gamma/r, \quad \Gamma = \frac{I}{2\pi(\sigma\nu\rho)^{\frac{1}{2}}}, \tag{15}$$

and the magnetic field $\boldsymbol{h}$ vanishes. The vorticity generated at the electrode is confined above it. The electric current vanishes in the bulk flow, and Ohm's law (5) is reduced there to $\nabla\Phi = \boldsymbol{v}\times\boldsymbol{B}_0$, so that the electric resistance is

$$R = \frac{\Phi(L)-\Phi(b)}{I} = \frac{B_0}{2\pi(\sigma\nu\rho)^{\frac{1}{2}}}\ln L/b. \tag{16}$$

Let us now take into account the correction due to viscous effects in the vortex core, but neglect radial and vertical velocity components, which is valid for large interaction parameters. This problem was solved directly by means of Bessel functions of the radius by Kalis & Kolesnikov (1980). However, the convergence of this method is very poor at large Hartmann numbers. Furthermore the authors assume that the current distribution in the electrode is not influenced by the fluid motion, which is not true in a strong magnetic field. It is then more simple to consider the Hartmann layer and the core of the flow separately, as was done by Hunt & Stewartson (1969) in a similar situation, mathematically identical for the bulk flow. Their problem can indeed be obtained from the present one by interchanging h and v and reflecting in the plane $z = a$. However the physical situation is quite different: the flow was restricted to a jet rotating around the electrode and the magnetic field decreased as $1/r$ in the former case, while the reverse situation occurs here. The classical method is to add and subtract (1) and (2) written in polar coordinates r, θ, z and to drop the second order z derivatives, which yields in a non-dimensional form

$$-M\,\partial(v+h)/\partial\zeta = D_\chi(v+h), \tag{17}$$

$$M\,\partial(v-h)/\partial\zeta = D_\chi(v-h), \tag{18}$$

where $\chi = r/a, \quad \zeta = z/a,$

$$v = (a/\Gamma)\,v_\theta, \quad h = (2\pi a/\mu_0 I)\,h_\theta, \quad \Phi = (2\pi a\sigma/I)\,\phi,$$

$$D_\chi = \partial/\partial\chi(1/\chi\,\partial/\partial\chi),$$

each of (17) and (18) is formally analogous to a time dependent diffusion equation for the quantities $v+h$ and $v-h$, the 'time' being either $-z/M$ or z/M respectively. The

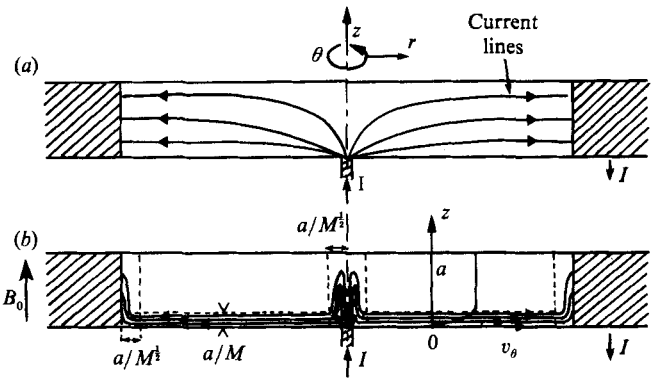

FIGURE 2. The electric current streamlines (*a*) without magnetic field, (*b*) in a strong magnetic field. The Hartmann layer, the outer layer parallel to the field and the vortex core are presented, as well as a vertical velocity profile.

boundary conditions for the bulk flow correspond to the upper part of the Hartmann layer and can be derived from (6)–(10).

$$(v+h)_{(\zeta=1)} = (v-h)_{(\zeta=1)}, \tag{19}$$

$$(v+h)_{(\zeta=0)} = -(v-h)_{(\zeta=0)} \quad \text{for } \chi < \lambda, \quad (v+h)_{(\zeta=0)} = 1/\chi \quad \text{for } \chi > \lambda, \tag{20}$$

where $\lambda = b/a$ is the non-dimensional radius of the electrode.

Analytical solutions can be obtained for $\lambda M^{\frac{1}{2}} \gg 1$ as in Hunt & Stewartson (1969) and for $\lambda M^{\frac{1}{2}} \ll 1$ as in Hunt & Williams (1968). In the former case, the layer parallel to the field arising from the edge of the electrode is much thinner than the radius of the electrode and can be considered as locally straight. In the latter case, this layer is replaced by a small region above the point electrode, the vortex core, where viscosity effects are important. Although our situation is between these two extremes, it is enlightening to write the solution for a point electrode

$$\left.\begin{aligned} v(\chi, \zeta) &= -1/\chi + \{\exp -M\chi^2/4\zeta + \exp -M\chi^2/4(2-\zeta)\}/2\chi, \\ h(\chi, \zeta) &= \{\exp -M\chi^2/4(2-z) - \exp -M\chi^2/4z\}/2\chi. \end{aligned}\right\} \tag{21}$$

The potential difference between the electrode and the circular frame at distance L (figure 1) can then be calculated from (5) and (4) by integration along the radius, and the result for $L \gg \lambda$ is

$$\phi(L, 0) - \phi(b, 0) = -M \ln L/b + \tfrac{1}{4}M \int_{\frac{1}{2}M\lambda^2}^{\infty} \frac{e^{-x^2}}{x}\, dx + \tfrac{1}{8}\, e^{-\frac{1}{8}M\lambda^2}. \tag{22}$$

A calculation taking into account the finite size of the electrode can be made by a simple numerical method, whose principle is the following. Starting at $\zeta = 0$ with $v+h = 1/\chi$, $\chi > \lambda$ and a guess for $\chi < \lambda$, for example $v+h = 0$, (17) is integrated to give the distribution of $v+h$ at $\zeta = 1$. This distribution can be considered as an initial condition for $v-h$ in (18) by means of (19). This equation can be then integrated, which leads to a new value of $v+h$ at $\chi = 0$, $\xi < \lambda$ (by (20)). This forward and backward process is repeated until the boundary conditions are no longer modified, which happens fairly quickly (a precision of 10^{-3} is obtained after three iterations of this process). The numerical method for integrating the diffusion equation is the standard explicit finite difference scheme. The profile of χv at the free surface

calculated by this method is represented in figure 4 and the variation of the electric resistance Φ/I with the magnetic field in figure 5. The difference with the results (21) and (22) is small, except in the region near the electrode edge.

The calculation is valid in the limit of very weak currents corresponding to large interaction parameters. Depending on the radius r that we consider, the flow contains different velocity scales $U(r) = \Gamma/r$ outside the vortex core. The corresponding interaction parameter $N(r) = (\sigma B^2/\rho)\, r^2/\Gamma$ increases steadily from a minimum value near the centre to a maximum at the radius of the box. The minimum is located at the radius of the vortex core, on the order of $a/M^{\frac{1}{2}}$ for weak currents, and the corresponding interaction parameter is

$$N_c = 2\pi\nu\sigma B_0\, a/I. \tag{23}$$

We can then expect that, when the current is increased, nonlinear effects will act first in the core and depend only on the parameter N_c. These effects must involve complex recirculating flows with a radial component that would broaden the core. Outside this core, the interaction parameter increases steadily and the flow should not be affected by advective effects. We can expect that the potential drop mostly occurs outside the vortex core for two reasons: the velocity is small inside the core, and the electric current can go through a large section of fluid instead of being confined to the Hartmann layer for larger radii. We can then write the electric resistance, by analogy with (16), as

$$R = \frac{B_0}{2\pi(\sigma\nu\rho)^{\frac{1}{2}}} \ln(L/r_0), \tag{24}$$

where r_0 is a characteristic radius of the core, that should depend only on the parameter N_0.

3.4. *Decaying vortices*

We consider a vortex generated by a short initial current pulse of duration τ. The driving force of the two-dimensional approximation can be obtained from (13), using axisymmetry

$$f = B_0 I/2\pi\rho a. \tag{25}$$

If this force dominates all other effects during the current pulse, the circulation of the generated vortex is

$$\Gamma_0 = (B_0 I\tau/2\pi\rho a). \tag{26}$$

After this initial stage the vortex should decay exponentially with a characteristic time t_H.

At the beginning of the current pulse, before the flow has time to build up, the current distribution in the fluid is the same as in the absence of a magnetic field, generating a vortex core with a radius on the order of the layer thickness a. However, in the very short typical time of the electromagnetic effects $\rho/\sigma B_0^2$ after the end of the pulse, the vortex core should take a new structure with a smaller size on the order of $a/M^{\frac{1}{2}}$, for low velocities. For higher velocities we can expect a broadening of the core due to secondary flows. As in the case of a steady vortex, this effect should depend only on the interaction parameter based upon the lengthscale $a/M^{\frac{1}{2}}$ and the velocity at the corresponding radius, which is now

$$N_d = 2\pi(\sigma\rho\nu)^{\frac{1}{2}} a^2/I\tau. \tag{27}$$

If we consider two vortices of opposite sign, the pair should move without deformation at velocity

$$v = (\Gamma_0/d)\exp(-t/t_H), \tag{28}$$

where d is the distance between the two electrodes and Γ_0 is given by (26). We have assumed that d is definitely larger than the core of each vortex. A vortex created near a straight lateral boundary should move in the same way, under the influence of the image vortex behind the wall.

4. The experimental results

4.1. *The steady vortex*

A steady current is injected at the box centre and returns through the frame. In the absence of a magnetic field we measure an electrical resistance equal to 0.56 mΩ. The distribution of electric potential in mercury is a solution of the Poisson equation, and is then analogous to the electrostatic potential near a conducting disk (because the conductivity is much larger in copper than in mercury). It can be calculated analytically if we assume that the mercury fills an infinite domain limited by the plane containing the bottom of the box, and the result is $R = \frac{1}{4}\sigma b = 0.19$ mΩ. If we add to this value the resistance of the copper part 0.13 mΩ, an excess of 0.24 mΩ still exists, and it must be imputed to contact resistance at the surface of the electrode. This value is reproducible, even after the mercury has been replaced.

When the magnetic field is applied, a smooth vortex is obtained (figure 3) and no fluctuations are observed on photographs, even at the highest current (400 mA) that we have used. We did not go beyond this value to avoid an excessive hollowing of the free surface near the vortex centre. If any velocity fluctuations exist at the surface, their relative amplitude is certainly smaller than 5×10^{-2}, considering the precision of the streak measurements. We did not observe any fluctuations of the electric potential, either, although we could certainly detect oscillations of relative amplitude as small as 2×10^{-3}. Therefore the flow appears to be very stable.

The profile of the angular momentum rv_θ obtained from photographs is plotted in figure 4. The vorticity $1/r\,\partial(rv_\theta)/\partial r$ is restricted to the neighbourhood of the electrode as it should be, and the momentum at large distances is equal to the theoretical value (relation (16)). Furthermore the profile near the centre is in good agreement with the more complete calculation of §3.3, when the electric current is small (< 50 mA). With larger currents, for example 200 mA, the vortex core is broadened. This effect is probably due to the radial transport of vorticity by secondary flows which are neglected in the linear calculation of §3.3. These secondary flows are directly revealed by the rarefaction of the visualization particles near the centre after a few seconds, which means that a weak (< 1 mm/s) radial outward motion exists there. However, we are not able to describe the structure of these secondary flows below the surface.

The increase of the electric resistance with the magnetic field is dramatic (figure 5), which corresponds to a remarkable feature. Without a magnetic field the resistance is mainly due to the fluid in the neighbourhood of the electrode where the current density is high. In a strong magnetic field the whole current flows only in the thin Hartmann layer, and the contribution of the regions far from the electrode decreases only logarithmically with the radius. For small currents, the agreement with (16) is fairly good and it is excellent with the numerical calculation (figure 5). This result can be considered as a direct measurement of the Hartmann-layer thickness inferred from its electrical resistance. The theoretical curve of figure 5 is obtained after adding the resistance of the copper part and the contact resistance measured without the magnetic field. The contact resistance is probably underestimated by this method, since the current lines are more confined near the edge of the electrode in the

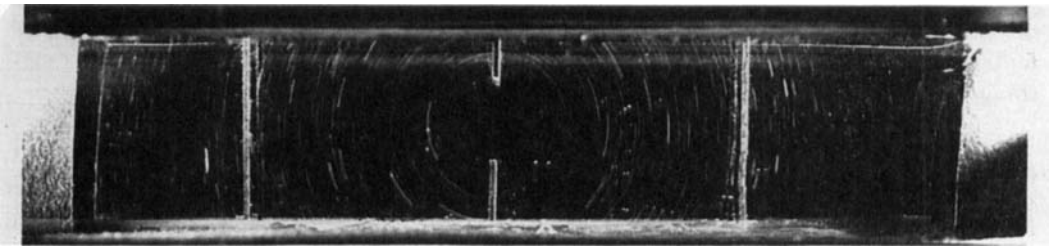

FIGURE 3. Photograph of the streak in a steady vortex. The band of the free surface is observed by means of a 45° mirror. $B = 0.48$ tesla, $I = 50$ mA, time of exposure 0.1 s.

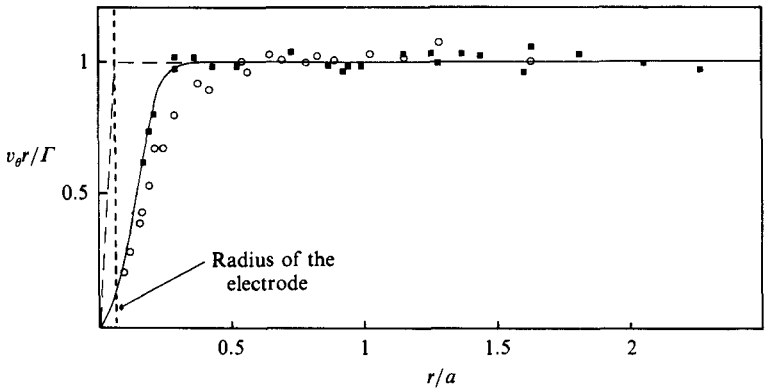

FIGURE 4. The non-dimensional momentum $v_\theta r/\Gamma$ versus the non-dimensional radius r/a, obtained from photographs, $B = 0.5$ tesla. ■, $I = 50$ mA; ○, $I = 200$ mA.

magnetic field, so that the current density is greater. One could explain by this effect that the experimental results for a current 6.5 mA are slightly (1%) above the theoretical ones.

For higher values of the current, the resistance is smaller, and this fact is consistent with the broadening of the core, as discussed at the end of §3.3. We have calculated the radius of the core r_0 inferred from the resistance by (24), and plotted it in figure 6 as a function of the inverse of the interaction parameter N_c, for a wide range of magnetic fields and currents. The collapse of the points near a single curve is a proof that the parameter N_c is indeed the relevant one to describe the advective effects in the vortex core. Notice that appreciable nonlinear effects appear only at really low values of N_c, which means that this vortex flow is not very sensitive to these effects.

4.2. *The decaying vortex*

When the current is switched off in the preceding experiments, the voltage decreases slowly, due to the vortex decay. In figure 7, the evolution of the electric potential is compared to the decay $\exp -t/t_H$ of a two-dimensional bulk flow, due to Hartmann friction only. The observed rate of decay depends on the initial velocity, related in turn to the driving current in the previous steady situation. In the case of strong magnetic fields and small initial currents, for which secondary flows must be negligible, we find a characteristic decay time of $0.91\ t_H$. This is illustrated by the dashed curve of figure 7, obtained for $B_0 = 0.48$ tesla and $I = 12.5$ mA. At the same

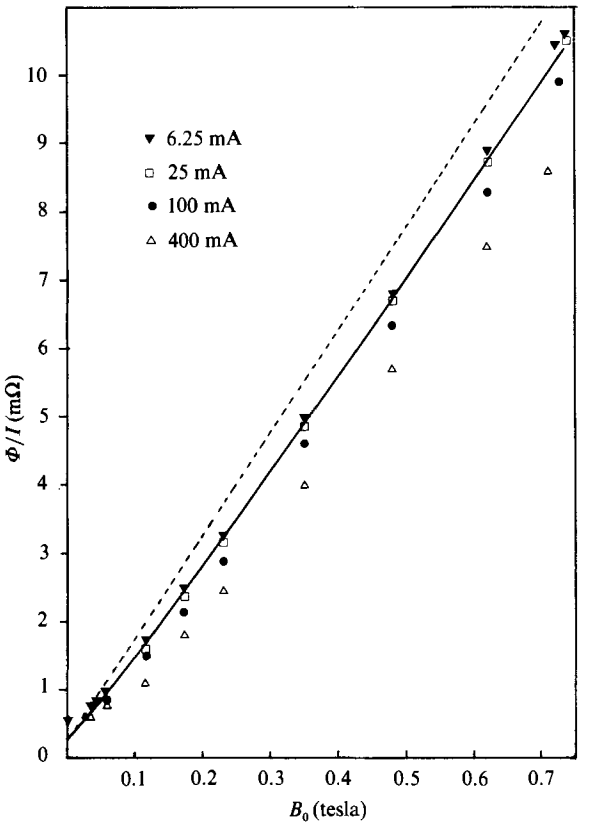

FIGURE 5. Increase of the electrical resistance with the magnetic field B_0 for different values of the current I. The theoretical result (relation (16)) for a two-dimensional vortex is represented by a dotted line and the result from the numerical solution of (17) and (18) is represented by a solid line.

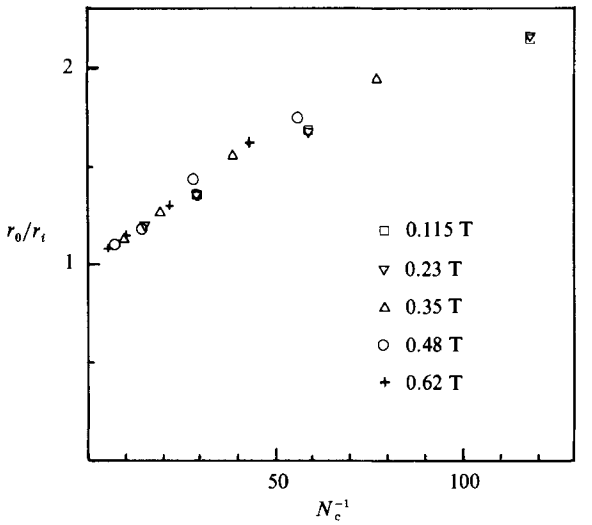

FIGURE 6. Core radius r_0 defined by (24) (and normalized by its value for a very small electric current) versus N_c, the interaction parameter of the vortex core. The current is between 0 and 0.4 A and the magnetic field is indicated in the figure.

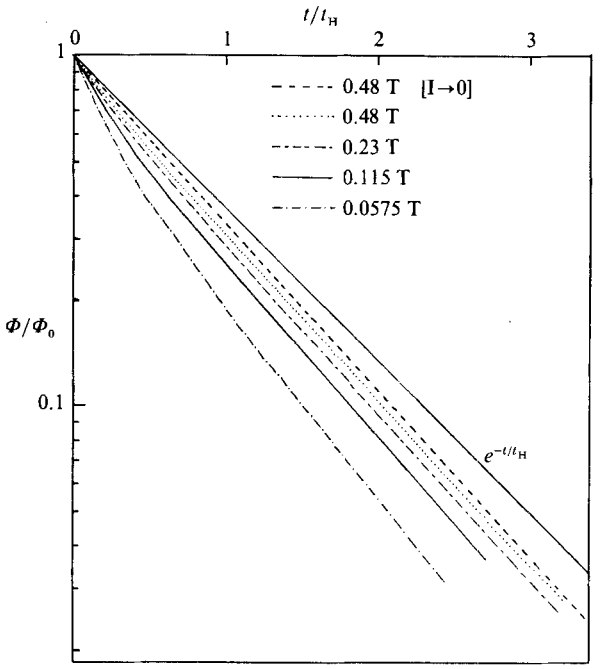

FIGURE 7. Decay of the electric potential Φ at the electrode (normalized by its initial value Φ_0) versus the non-dimensional time t/t_H after the steady current is switched off. The Hartmann decay is represented by a solid line and the experimental result for a small initial current (12.5 mA) and $B_0 = 0.48$ tesla by a dotted line. The other curves are obtained with an initial current 50 mA and different values of the magnetic field.

time the decay rate of the velocity outside the core, measured from photographs, corresponds well to the Hartmann friction. Therefore the increased decay of the potential is due to a broadening of the core by viscous diffusion during the decay. When advective effects are influential (i.e. for small magnetic fields or large initial electric current), the rate of decay is faster. This fact can be explained by the broadening of the core due to the advective transport. Notice that as the vortex becomes weaker, the decay rate is close to $0.91\ t_H$, probably because the secondary flows have disappeared. This behaviour is shown in figure 7 for an initial current 50 mA and decreasing values of the magnetic field.

4.3. *Isolated vortex generated by a current pulse*

Electric pulses of 2 A during a time $\tau = 0.3$ s are injected in motionless mercury, and the magnetic field is 0.5 or 1 tesla. Velocity profiles are obtained from successive photographs with a period of 0.5 s, starting at a time origin chosen at the middle of the pulse. It is especially necessary for the free surface to be extremely clean. Indeed the fluid is initially at rest, so that the possible thin film of impurities is not broken by previous motion. Therefore, the reproducibility of the results was carefully checked, and the pulse was chosen to be sufficiently strong to obtain a maximum velocity, at least a few cm/s. Since the driving force is applied during a short time, it must be intense to get this typical velocity, and a linear regime in the core was never obtained, by contrast with the steady vortex.

The angular momentum rv_θ, represented in figure 8, does not depend on the radius at large distances, but it is surprisingly about 10% smaller than the theoretical value

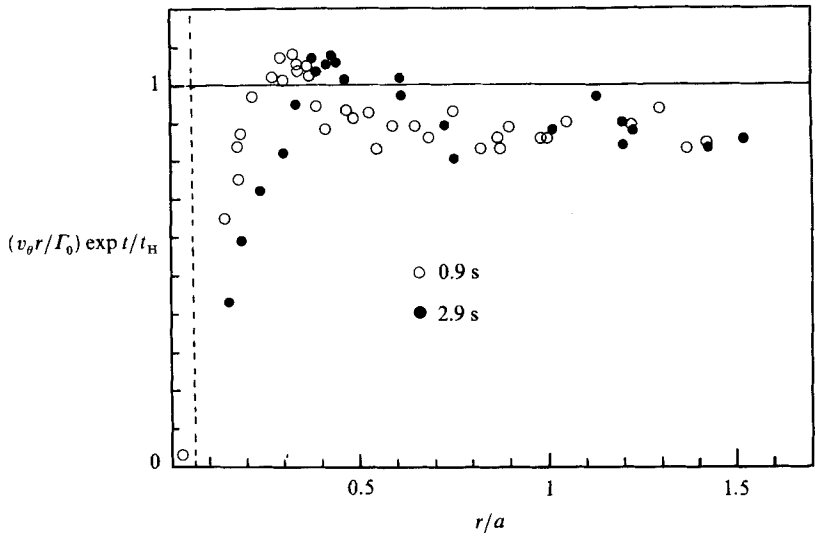

FIGURE 8. Non-dimensional momentum $(v_\theta r/\Gamma_0)\exp t/t_H$ versus r/a for a vortex generated by a current pulse, $t = 0.9$ s and $t = 2.9$ s after its production. Magnetic field 1 tesla, time of exposure 0.1 s.

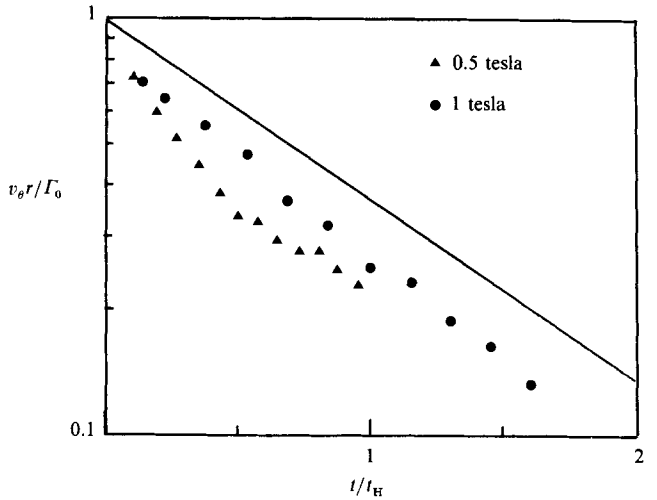

FIGURE 9. Decay of the non-dimensional momentum $v_\theta r/\Gamma_0$ for $r/a = 1$, $B = 0.5$ and 1 tesla compared to the Hartmann decay (solid line).

Γ_0. Therefore there is a strong dissipation effect during the current pulse, even at a large distance from the electrode. The vorticity profile in the core is different from that in the steady case: the central region of positive vorticity is surrounded by a screen of negative vorticity. This feature is probably due to some radial transport of angular momentum by the strong secondary flows during the current pulse. The interaction parameter N_d is equal to 0.12 for the two cases, so it is not surprising to have rather important nonlinear effects in the core. The subsequent evolution, indicated on figure 9 at a radius $r = a$ far outside the core, corresponds to the Hartmann decay for $B_0 = 1$ tesla. However the decay is somewhat faster at the beginning for $B = 0.5$ tesla, which could be due to some residual three-dimensional

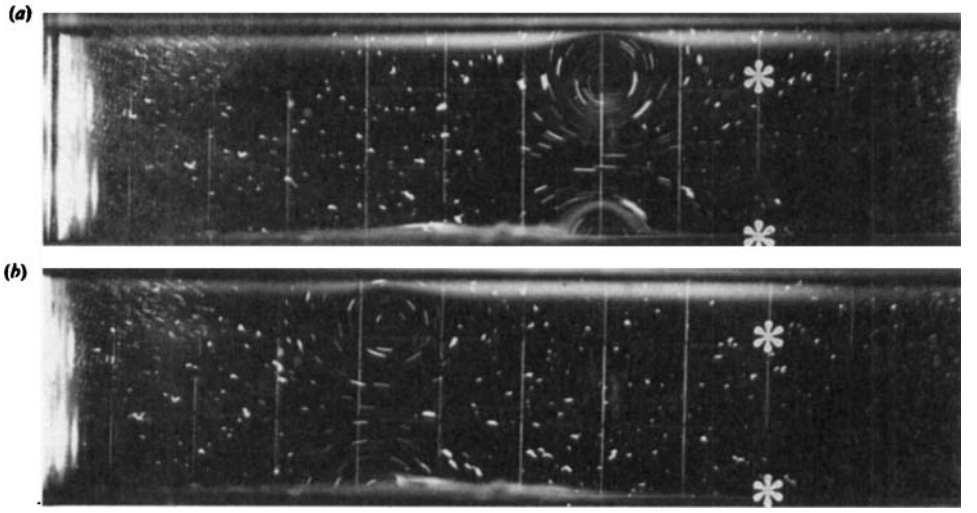

FIGURE 10. Photograph of a vortex pair produced by a current pulse between two electrodes 1.4 s (*a*) and 3.9 s (*b*) after its creation. The initial position is indicated by the stars; the magnetic field is 1 tesla, time of exposure 0.05 s.

effects persisting far from the core. This result is surprising, as well as the discrepancy of the initial circulation with theory, but it is reproducible and not due to a dirty surface. In all cases, there is also a slow diffusion of the vortex core shown in figure 8.

4.4. *A vortex pair*

A vortex pair is generated by two electrodes at a distance $d = 2$ cm (using the square box). It is created at 3 cm from one wall and travels towards the opposite wall, and the time of observation is limited by the collision of the pair with this latter wall. The velocity of translation is obtained from successive photographs, as shown in figure 10, taken with a time interval of 0.5 s. The initial value of this velocity, as well as the decay are always in good agreement with (28) (figure 11) for the two values of the magnetic field (0.5 and 1 tesla) that we used. (The rate of decay increases a little at the end, and this behaviour corresponds to a slight increase of the distance between the vortices, due to the interaction with the image vortex pair behind the front wall.) The velocity at the middle of the pair, measured from the particle streaks is equal to four times the speed of translation, as it should be for point vortices. Thus the two-dimensional approximation is more precise when the vorticity is advected away from the electrodes, rather than localized as in the previous section. The reason is probably that the relevant interaction parameter should be calculated with the distance between the two vortices and is larger than N_d.

4.5. *Interaction of a vortex with the wall*

We have produced a single vortex in the square box at a distance 3 cm and 1 cm from one of the sides, while the vortices of §4.3 were created at the centre. At 3 cm we observe a translating motion in good agreement with (26), for the pair formed with the image vortex behind the wall. However at 1 cm the behaviour is quite different: a detachment of the lateral boundary layer occurs, and a new vortex of opposite sign is created, as shown in figure 12. The resulting pair of two unequal vortices stays in the neighbourhood, with a rotating motion. We did not explore the conditions for the occurrence of this detachment, which deserves further investigation.

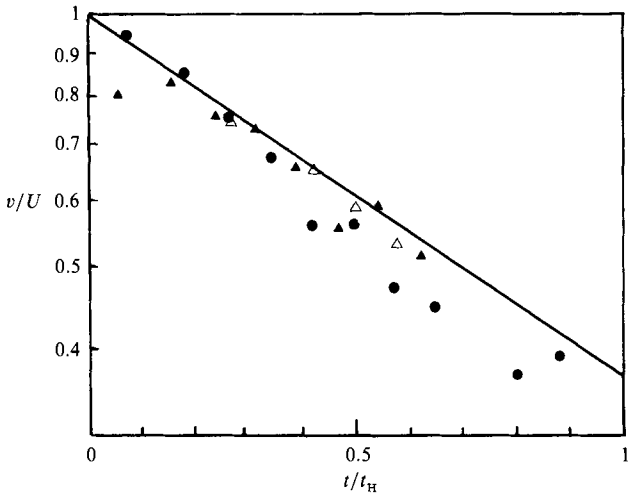

FIGURE 11. The decay of the vortex pair, ●, $B = 1$ tesla, translation velocity; ▲, $B = 0.5$ tesla, translation velocity; △, $B = 0.5$ tesla, velocity at the centre of the pair divided by 4. The Hartmann decay is represented by a solid line.

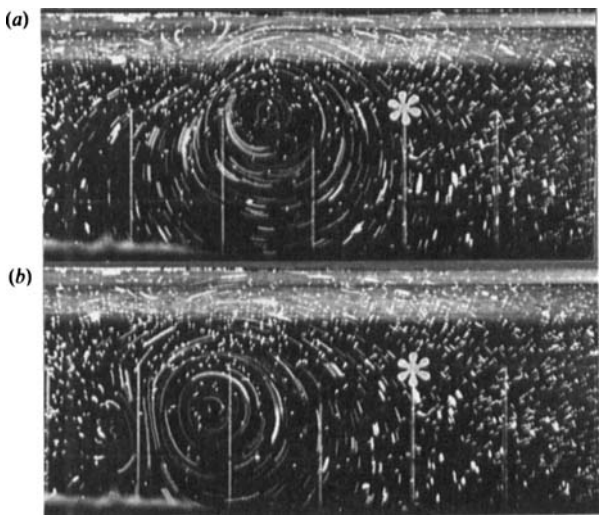

FIGURE 12. Production of a secondary vortex by boundary layer detachment. The main vortex is generated by a pulse of 2 A during 0.1 s at the location represented by a star. The wall is at the upper edge of each photo. Magnetic field 1 tesla, time of exposure 0.2 s (*a*) time $t = 1.4$ s; (*b*) time $t = 2.4$ s.

5. Conclusions

The electrically driven steady vortex is a relatively simple MHD flow which seems not to have been studied previously. There is a close theoretical similarity between this flow and that of Hunt & Stewartson (1969), although the physical situation is different. Excellent agreement with the asymptotic theory for high Hartmann numbers is obtained when the current is weak. In particular, the confinement of all the electric currents to the thin Hartmann layer is confirmed by the dramatic increase in the electric resistance as the magnetic field is stronger. For higher

currents, a broadening of the vortex core is probably due to recirculating flows, which are not taken into account by the linear asymptotic theory. We show that this effect depends only on the interaction parameter N_c based upon the lengthscale $a/M^{\frac{1}{2}}$ of the vortex core and the corresponding velocity.

In most cases, the flow structures decay exponentially with the characteristic time of Hartmann friction t_H, outside the vortex cores. This result could be expected since the Reynolds number of the Hartmann layer Re/M was always well under the value 250, below which the Hartmann layer is found to be laminar in ducts. Yet, it seems that the Hartmann friction was measured here for the first time in decaying flow structures. A lateral diffusion by viscosity effects is observed in the vortex core, as well as a broadening by nonlinear effects for very small values of the local interaction parameter. Notice also that the dissipation far from the core is somewhat stronger than expected for the vortex created by a strong initial current pulse in a moderate magnetic field (0.5 tesla). We do not explain this result, which could be due to the persistence of some three-dimensional perturbations.

An interesting application of these electrically driven flows is the production of various two-dimensional inertial flow at high Reynolds number. A great variety of steady or unsteady forcings can be obtained by dispatching an electric current in a network of many electrodes, as in Sommeria (1986) or Verron & Sommeria (1987). The main elementary MHD processes existing in this kind of device have been studied here. It appears that the flow can be well described by the two-dimensional Navier–Stokes equation with a vorticity production on the electrodes and the Hartmann friction, when the interaction parameter is not too small. The vortex cores are regions with a small scale and high velocity, hence the most influenced by three-dimensional effects. However these effects tends to disappear when the vorticity is advected away from the electrode, as in the vortex pair. Notice finally that the flow can be influenced by a vortex production due to the detachment of the lateral boundary layer.

The author has benefited from useful comments by R. Moreau, and from the support of R. Bolcato for the realization of the experimental device.

REFERENCES

ALEMANY, A., MOREAU, R., SULEM, P. L. & FRISCH, U. 1979 Influence of an external magnetic field on homogeneous turbulence. *J. Méc. (Paris)* **18**, 277.

BAYLIS, J. A. 1971 Experiments on laminar flow in curved channels of square section. *J. Fluid Mech.* **48**, 417–422.

BRANOVER, H. 1978 *Magnetohydrodynamic Flows in Ducts*. Halsted.

BRANOVER, H. & GERSHON, P. 1979 Experimental investigation of the origin of residual disturbances in turbulent MHD flows after laminarization. *J. Fluid Mech.* **94**, 629–647.

GEL'FGAT, YU. M., KIT, L. G., PETERSON, D. A. & TSINOBER, A. B. 1971 Realization of the laminar regime in magnetohydrodynamic flow in an annular channel at high Reynolds number. *Magnitnaya Gidrodinamiks*, **3**, 35–42.

HUA, H. M. & LYKOUDIS, P. S. 1974 Turbulent measurements in a magneto-fluid mechanics channel. *Nucl. Sci. Eng.*, **54**, 445.

HUNT, J. C. R. & LEIBOVICH, S. 1967 Magnetohydrodynamic flow in channels of variable cross-section with strong transverse magnetic fields. *J. Fluid Mech.* **28**, 241–260.

HUNT, J. C. R. & MALCOLM, D. G. 1968 Some electrically driven flows in magnetohydrodynamics: Part 2. *J. Fluid Mech.* **33**, 775–801.

HUNT, J. C. R. & SHERCLIFF, J. A. 1971 Magnetohydrodynamics at high Hartmann number. *Ann. Rev. Fluid Mech.* **3**, 37–62.

HUNT, J. C. R. & STEWARTSON, K. 1969 Some electrically driven flows in magnetohydrodynamics. Part 3. *J. Fluid Mech.* **38**, 225–242.

HUNT, J. C. R. & WILLIAMS, W. E. 1968 Some electrically driven flows in magnetohydrodynamics. Part 1. *J. Fluid Mech.* **31**, 705–722.

KALIS, KH. E. & KOLESNIKOV, YU. B. 1980 Numerical study of a single vortex of a viscous incompressible electrically conducting in an homogeneous axial magnetic field. *Magnitnaya Gidrodinamika* **2**, 57–61.

KAPILA, A. K. & LUDFORD, G. S. S. 1977 MHD with inertia: flow over blunt obstacles in channels. *Intl J. Engng Sci.* **15**, 465–480.

KOLESNIKOV, YU. B. & TSINOBER, A. B. 1974 Experimental investigation of two-dimensional turbulence behind a grid. *Isv. Akad. Nauk. SSSR Mech. Zhid. i Gaza* **4**, 146.

LEHNERT, B. 1952 Experiments on non-laminar flow of mercury in presence of a magnetic field. *Tellus*, **4**, 63–67.

LIELAUSIS, O. 1975 Liquid metal magnetohydrodynamics. *Atomic Energy Rev.* **13**, 527.

LOCK, R. G. 1955 The stability of the flow in an electrically conducting fluid between parallel planes under a transverse magnetic field. *Proc. R. Soc.* A **233**, 105–125.

MALCOLM, D. G. 1970 An investigation of the stability of a magnetohydrodynamic shear layer. *J. Fluid Mech.* **41**, 531–544.

SHERCLIFF, J. A. 1965 *A Textbook of Magnetohydrodynamics.* Pergamon.

SHERCLIFF, J. A. 1975 Some duct flow problems at high Hartmann number. *Z. angew. Math. Phys.* **26**, 537–547.

SOMMERIA, J. 1985 Two-dimensional behaviour of electrically driven flows at high Hartmann numbers. 4th Beer Sheva Seminar on MHD flows and turbulence. *AIAA Prog. ser.* **100**.

SOMMERIA, J. 1986 Experimental study of the two-dimensional inverse energy cascade in a square box. *J. Fluid Mech.* **170**, 139–168.

SOMMERIA, J. & MORREAU, R. 1982 Why, how, and when, MHD turbulence becomes two-dimensional. *J. Fluid Mech.* **118**, 507–518.

TABELING, P. & CHABRERIE, J. P. 1981 Magnetohydrodynamic secondary flows at high Hartmann numbers. *J. Fluid Mech.* **103**, 225–239.

TABELING, P. & TRAKAS, C. 1984 Structures spiralées dans une instabilité de Taylor en présence de champ magnétique. *J. Phys. Paris* (*Lett.*) **45**, L159–L167.

VERRON, J. & SOMMERIA, J. 1987 Numerical simulation of a two-dimensional turbulence experiment in magnetohydrodynamics. *Phys. Fluids* **30**, 732–739.